International Journal of Theoretical and Applied Research (IJTAR)
ISSN: 2812-5878

Homepage: https://ijtar.journals.ekb.eg

Original article

Catalytic Assessment of Nickel based Catalyst for Methane Synthesis from Syngas in a Fluidized Bed Reactor

Mohamed ElNahrawy [1,*], Delvin Aman [2], Tamer Zaki [2], Sara Mikhail [2], Shaaban Nosier [1], Alhassan Nasser [1]

[1] *Chemical Engineering Department, Faculty of Engineering, Alexandria University, Alexandria, Egypt.*
[2] *Petroleum Refining Department, Egyptian Petroleum Research Institute, Cairo, Egypt.*

ARTICLE INFO

Received 17/05/2022
Revised 28/06/2022
Accepted 03/07/2022

Keywords

CO Methanation
SNG
Rice Husk
Fluidized bed reactor
CH4 Production

ABSTRACT

Synthetic natural gas (SNG) has attracted significant attention over the past years due to its critical role in the future energy mix where it can be produced from multiple sources, including coal, wastes & biomass. Carbon monoxide (CO) methanation is considered one of the major SNG production routes. Nickel oxide catalyst supported on silica extracted from risk husk was prepared using wet impregnation method and characterized using different techniques including XRD, N_2 Adsorption, Atomic absorption, XRF & TPR. Distinctively from most of the published previous work, The catalyst performance in progressing CO Methantion reaction was tested in a bubbling fluidized bed continuous flow reactor system at the stoichiometric H_2:CO ratio of 3:1 in absence of any other feed constituents. The catalytic runs were conducted at atmospheric pressure, in the temperature range between 200-450^{o}C and at fluidization velocity equal to four times the minimum fluidization velocity (U_{mf}). CO conversion, CH_4 selectivity & CO_2 Selectivity were calculated for all runs. Based on the assessment of catalytic runs, fluidized bed reactor system proved to be efficient in ensuring adequate temperature control and uniformity for CO methanation. Optimal results of 97% CO conversion, 81% CH_4 selectivity and 21% CO_2 selectivity were achieved at operating conditions of temperature of 450^{o}C, pressure of 1 bara & superficial velocity of 4 U_{mf}. Recommendations for future work in terms of catalyst development and operating conditions were also made based on the results achieved.

Graphical abstract

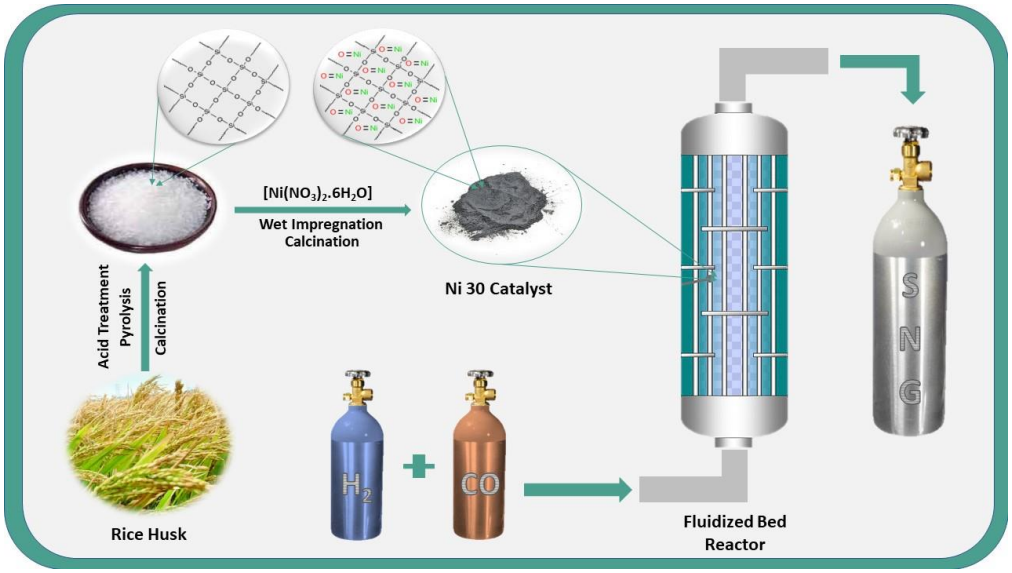

∗ *Corresponding author.*
E-mail address: mohamedelnahrawy93@gmail.com

DOI: 10.21608/IJTAR.2022.138960.1001

Special issue "selected papers from the International Annual Conference on Basic and Applied Science (IACBAS-2022)"

1. Introduction

Demand for synthetic natural gas has increased in recent years as it serves multipurpose in managing the global energy dual challenge of higher global energy demand with fewer emissions[1][2]. On one hand, natural gas is considered a less environmentally polluting fossil fuel [3]. It also possess a major advantage of fossil fuels which is energy availability on demand with no intermittency issues similar to those crippling alternative energies like wind & solar. On the other hand, SNG can be produced from Syngas, which can either be obtained from Coal, municipal waste, biomass or even waste plastics[1], [4]. In other words, SNG offers an industrial route to utilize either emissions intensive fuel sources or wastes into fewer emissions energy source. Moreover, SNG takes full advantage of the existing transport & end usage infrastructure of natural gas [5], which is already providing a significant portion of the global energy demand.

Syngas methanation has been intensively studied on the lab scale and a few industrial facilities are already operational. Various metallic catalysts were studied for CO methanation including Pt, Ru, Rh, Fe, Ni & Co [6]. The activity of metallic catalysts were found to be in the following order Ru>Fe>Ni>Co whereas the selectivity towards methane production was found to be Ni>Co>Fe>Ru [6]. Nickel oxide is one of the most widely used catalysts for CO methanation due to its high activity, relatively economic production costs and high Methane selectivity [5]. Unsupported nickel catalyst have considerable limitations in methanation reaction as they are prone to deactivation through thermal sintering and carbon deposition [7][8]. Catalytic supports are a very active area of research for CO methanation reactions [5]. This is because the metal-support interaction can influence the catalytic performance through altering catalyst activity and metal dispersion [9] [8] . Different supports have been explored over the past years including alumina and cerium. Both of which have their own shortcomings when employed as a catalyst support for this highly exothermic reaction [10]. Supports are crucial for CO methanation since they provide better stability to the catalyst and help combat sintering and catalytic deactivation specially in the highly exothermic Methanation reactions. Among different supports explored for CO methanation, silica is proven to be an attractive choice owing to its high thermal stability availability and low production cost.

A global push towards a circular economy, sustainability in energy production and waste products utilization alongside with maximizing resources utilization favors using more eco-friendly materials in various industries. In this work, silica produced from rice husk is explored as an effective cost-efficient environmentally friendly catalyst support for CO methantion reaction.

Efficiently managing the aggressive exothermic nature of the CO methanation reaction is the cornerstone to successful scale up and commercialization [11]. Controlling the temperature rise inside the reactor on a large scale can be extremely challenging. To get a sense of the expected temperature rise, a conventional syngas fed to a single adiabatic reactor at a temperature of 250-300ºC could result in an adiabatic temperature of 900ºC [12].

Currently, two main designs are deemed suitable for commercial scale CO methanation being a series of adiabatic intercooled fixed bed reactors and a fluidized bed reactor system [12]. Fixed bed reactors require catalysts of very high thermal stability since temperature rise over the reactor bed can reach up to 700ºC and suffer from poor temperature distribution and potential for hotspots generation [13]. Fluidized bed reactors are an excellent choice for CO methanation, which is an extremely exothermic reaction owing to the fact that they have a much higher efficiency in heat exchange, compared to fixed beds, and better temperature distribution & control [14], due to the turbulent gas flow and rapid circulation.

Most experimental research work conducted on CO methanation is either done on selective CO methanation or in presence of an inert gas. In selective CO methanation the H_2/CO ratio is considerably higher than the stoichiometric ratio of 3:1 in addition to presence of other species in the reactant stream, most commonly CO_2. Selective methanation is usually done for the applications of syngas cleanup for Ammonia synthesis and recently for Proton-Exchange Membranes (PEM) fuel cells so it is usually a CO cleanup process from a stream rather than CO utilization for SNG production [15]–[17]. The work focusing on SNG production usually utilizes a percentage of an inert gas in the feed stream to aid in the removal of heat of reaction produced to avoid temperature hotspots in the fixed bed reactors usually utilized in this kind of work.

On a commercial scale, it is not economical to use a significant percentage of an inert gas within the process stream as this will increase operating costs for utilizing such high volumes of inert gases plus it will add also to the energy requirement for heating the inert gas prior to introduction to the reactor unnecessarily.

The essence of this work is to assess the adequacy of semi-pilot scale bubbling fluidized bed reactors in SNG production from a pure H_2/CO gas mixture with Stoichiometric feed ratio while maintaining decent temperature control despite the extremely exothermic nature of the reaction as a step forward in the journey of technology commercialization

2. Materials and Methods

2.1. Catalyst preparation

Silica was produced from rice husk by first rinsing the rice husk in 2% solution of HCl for 2 days. Pyrolysis of rice husk followed the acidification step where rice husk was heated to 900ºC in inert atmosphere of nitrogen. After that, the obtained powder was calcined at 900ºC in presence of purified air stream. The prepared silica was denoted RH-Silica.

To prepare the NiO catalyst, wetness impregnation method was used where the required weight of Nickel nitrate powder ($Ni(NO_3)_2.6H_2O$) was dissolved in distilled water before adding the required weight of RH-

Silica to the solution. The solution was continuously stirred for 45 minutes before being heated to 80ºC while continuously stirring the solution using a magnetic stirrer for 3 hours. The obtained gel is then dried overnight at 120ºC in an oven.

The produced powder is then calcined in flowing hot air at 450ºC for 5 hours with an incremental temperature increase of 10ºC/minute.

The prepared catalyst was denoted Ni30 representing the weight percentage of NiO in the prepared catalyst powder.

2.2. Catalyst Characterization

The morphology of the prepared sample was identified by Shimadzu (Japan)-X-ray diffraction (XRD) with a Cu Kα (λ = 1.5406 Å) radiation at a 40 kV voltage and current of 40 mA. . The surface area and pore volume were determined by USA-NOVA 3200 at - 196◦C. Temperature programmed reduction of prepared calcined sample was performed using ChemBet 3000, Quantachrome (USA). Chemical analysis of prepared silica was performed using X-ray fluorescence technique utilizing S8 TIGER Series 2 device, Bruker, Germany after burning 1 gram of prepared sample 1000ºC till constant weight Is achieved. The weight loss due to the removal of moisture and adsorbed gases was (0.870 wt.%). The impregnated NiO weight percentage in the catalyst was determined by Flame Atomic Absorption Spectrophotometer (AA-6300, Shimadzu).

2.3. Catalytic testing

The performance of the prepared Ni30 catalyst was tested in a continuous fluidized bed reactor system as illustrated in Fig. 1.

The reactor is made of stainless steel with an internal diameter of 2.54 cm and length of 1 m. The bottom section of the reactor entails a mesh support (5 micron mesh size) to support the catalytic bed and to aid in feed gas distribution to the reactor.

The mid-section of the reactor is of a uniform diameter. The reactor is equipped with a conical shaped disengagement section with marginally larger diameter to reduce the fluid's velocity with an aim of settling any carried over catalyst particles with the product stream.

The gaseous product leaving the reactor is then introduced to a gas-solid separation Cyclone to separate any potentially fugitive catalytic particles that could have been carried over as a result of either excessively high superficial gas velocities within the fluidized bed or due to catalytic particles attrition.

The clean gaseous produced gases are fed to a double pipe water-cooled heat exchanger to condense the produced water from the reaction in the cold trap before feeding the non-condensable gaseous product stream to a thermal-type mass flow meter and eventual disposal of the gas stream to a safe location.

Inside reactor, the following reactions are expected to be taking place with various extents of progression.

$$3H_2 + CO \leftrightarrow CH_4 + H_2O \quad \Delta H - 206\ KJ.mol - 1 \quad (1)$$

$$CO + H_2O \leftrightarrow CO_2 + H_2 \quad \Delta H + 41.2\ KJ.mol - 1 \quad (2)$$

The first reaction is the main reaction and is strongly exothermic, hence reactor selection is of paramount importance to ensure uniform bed temperature and efficient heat removal from the reaction media to effectively control the reaction temperature and prevent temperature runaway. The strong exothermic nature of the CO methanation reaction renders the fluidized bed reactor an attractive choice of reactor owing to its superior heat transfer properties leading to bed temperature uniformity and efficient heat removal.

The second reaction, being a side reaction, is the water gas shift reaction that favors the production of CO_2 from CO at the expense of CH_4. Catalyst's ability and reaction conditions are the main tools to maximize the extent of methanation reaction whilst minimizing CO_2 production through water gas shift side reaction.

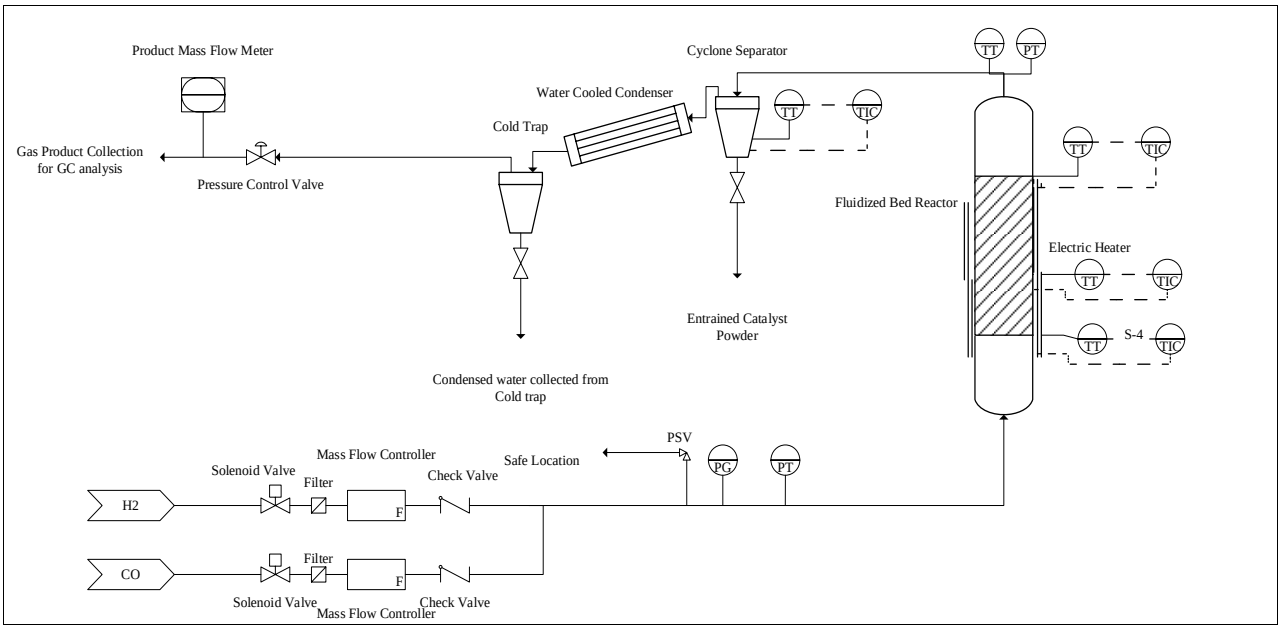

Figure 1. Schematic representation of the fluidized bed reactor system used for catalytic testing

Forty-Five grams of the catalyst were loaded into the reactor and reduced in situ at 500ºC for 2 hours in continuous Hydrogen flow of 2 Standard Liters Per Minute (SLPM). Minimum fluidization velocity (U_{mf}) of the catalyst was experimentally determined using a transparent plexi-glass cylinder having the same internal diameter as that of the reactor. The catalytic experiments were carried out at a fluidization velocity of 4 U_{mf} corresponding to 2 SLPM. The decision to test the catalytic reactor at a relatively high fluidization velocity is to assess the system's ability to withstand the significant heat generation expected from the reaction while maintaining a constant bed reaction temperature. The temperature range explored through the catalytic runs encompassed the temperatures between 200 & 450ºC. All catalytic runs were performed at atmospheric pressure with a H2/CO ratio of 3:1 in the mixed feed gas introduced to the reactor. The produced gases were analyzed using Thermo-Fischer ultra-trace Gas Chromatograph utilizing Thermal conductivity detector (TCD) to determine CO conversion, CO_2 selectivity, CH_4 Selectivity & according to the following equations.

$$\text{CO Conversion \%} = \frac{\text{Moles CO in-Moles CO out}}{\text{Moles CO in}} \text{X } 100$$

$$CH_4 \text{ Selectivity \%} = \frac{\text{Moles CH4 out}}{\text{Moles CO in-Moles CO out}} \text{X } 100$$

$$CO_2 \text{ selectivity \%} = \frac{\text{Moles CO2 out}}{\text{Moles CO in-Moles CO out}} \text{X } 100$$

3. Results and Discussion

3.1. XRD

X-ray diffraction pattern shown in figure 2 showed broad peak appeared at 2 theta= 21.4° that belong to non-crystalline silicon oxide (JCPDS 29-0085), which is typical for amorphous solids. This observation confirmed the absence of any ordered crystalline structure [18].

The XRD pattern of NiO exhibited shows five diffraction peaks at 2θ of 37.18°, 43.12°, 62.88°, 75.24°, and 79.23°, which corresponded well with the literature of the card (JCPDS 78-0423) XRD pattern.

High intensity and broad spectrum width in XRD spectra of NiO confirmed their well grain size, and the detection of no other peak related to impurity further confirmed their high purity and crystallinity [19], [20].

The XRD pattern clarifies the absence of Ni (III) oxide, as a result for carrying out the calcination step at temperature higher than temperature of 400°C [21].

3.2. BET

For RH-Silica samples, Full Adsorption-desorption isotherms are determined at -196°C. Fig. 3 shows that the adsorption was followed up to the saturation whereas the desorption was continued till the closure of the hysteresis loops, both of the isotherms are obeying the BET equation in the relative pressure range 0.05-0.35.

The nitrogen adsorption of the RH-Silica and NiO supported on silica samples started from low pressures as seen in Fig. 3, where it indicates that the adsorption isotherm is related to both of type I and type II according to the IUPAC classification [22], which reveals the presence of pores having micro porosity features. The isotherms of the samples are exhibiting H3 hysteresis loop. This type indicates the presence of non-rigid aggregates (assemblage of particles which are loosely coherent) of plate-like particles giving rise to slit-shaped pores [23]. Such non-rigid pores resulting in decreasing the pressure of loop closing, i.e. the hysteresis ended at P/P° 0.25. This low-pressure hysteresis usually associated with the swelling of the non-rigid pores [24].

As a result of metal dispersion on catalytic supports, the surface area tends to either decrease as a result of pores blockage or increase if the metallic dispersion is high and no pore blockage has taken place. Table 1 suggests that surface area increased from 161.91m2 /g to 344.09m2 /g after the loading process with 30wt.% nickel oxide.

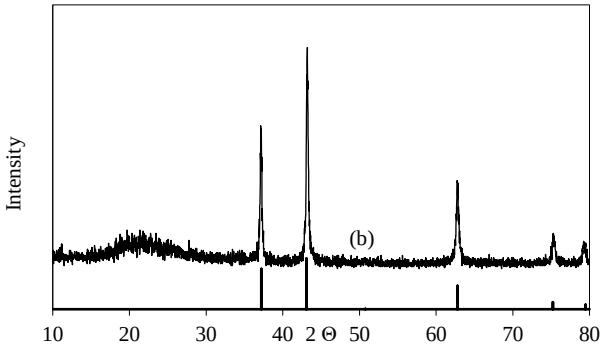

Figure 2. XRD patterns for (a) JCPDS 78-0423 & (b) Ni30 sample

This could be attributed to the formation of highly porous NiO agglomerates resulting in creation of new micropores as well as splitting of existing pores by NiO aggregates[25] [26].This is evident, as average pore size has decreased from 7.38 nm in case of RH-Silica to 6.08 nm in case of Ni30 Catalyst while total micro pore volume increased from 0.0124 to 0.5118 cm^3/g. NiO loading percentage was estimated against the target value of 30% Wt. using atomic absorption technique as shown in table 1.

Table 1. physiochemical properties (BET Surface area, Pore Volume & pore size) & NiO weight percentage determined by atomic absorption of RH-Silica & Ni30 samples

Sample	*Surface Area (m^2/g)*	*Pore Volume (cm^3/g)*	*Pore Size (nm)*	*micro pore volume (cm^3/g)*	*NiO weight percent*
RH-silica	161.91	0.2989	7.38	0.0124	0
Ni30	344.09	0.5234	6.08	0.5118	29.9

3.3. XRF

The chemical analysis of the prepared RH-Silica sample as determined using XRF analysis is shown in table 2

Table 2. Chemical analysis of RH-Silica sample as determined using XRF technique

Component	*Weight Percentage*
SiO_2	99.948
Al_2O_3	0.008
CaO	0.012
Na_2O	0.004
K_2O	0.002
MgO	0.001
Fe_2O_3	0.021
TiO_2	0.003
P_2O_5	0.001

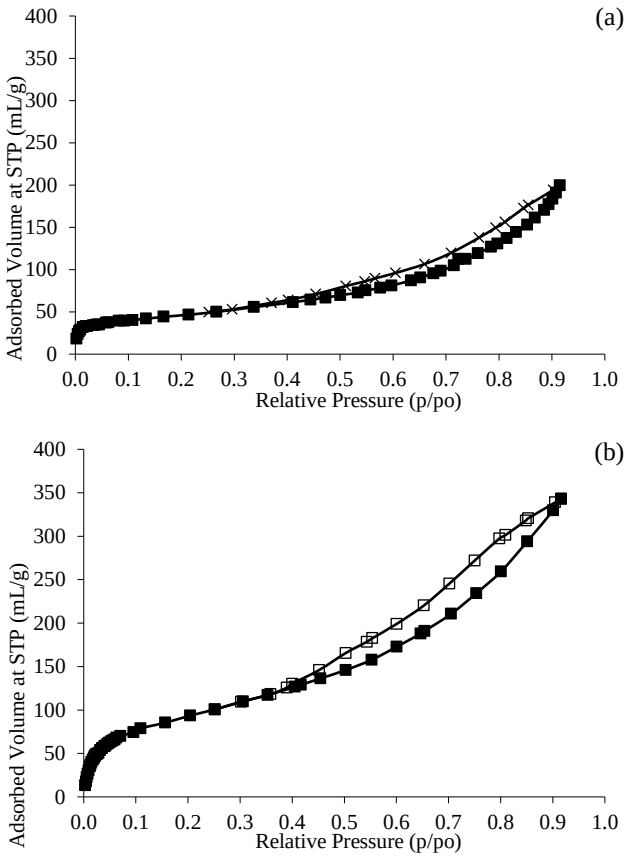

Figure 3. RH-Silica (a) & Ni30 (b) Adsorption Isotherms

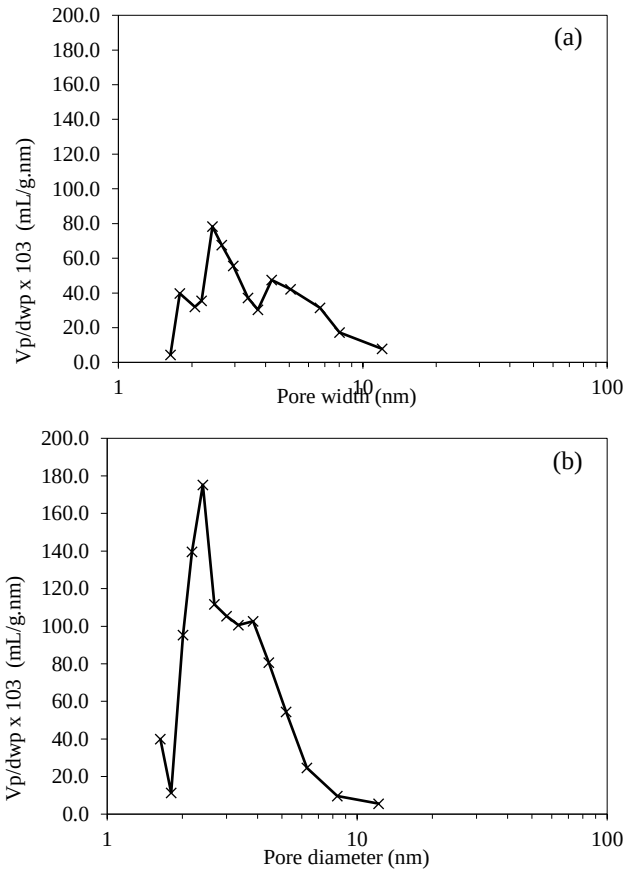

Figure 4. RH-Silica (a) & Ni30 (b) Samples Pore size distribution

3.4. TPR

In the TPR results of Ni30 catalyst displayed in Fig. 5, a distinct reduction peak at 450ºC is observed.

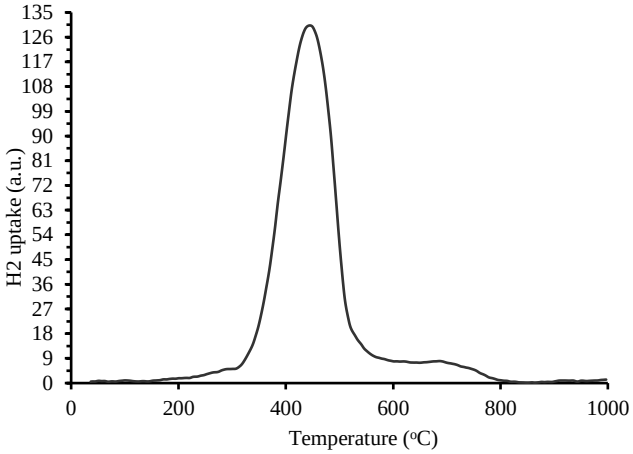

Figure 5. TPR Profile for Ni30 sample

Literature suggests that presence of a metal-support interaction generally leads to a reduction in the metallic oxide reducibility which explains the lack of a reduction peak at 300ºC corresponding to unsupported NiO reduction [27]–[30]. The lack of any reduction evidence at 200 ºC confirms the XRD conclusion of Ni III species absence [31]. The distinct reduction peak at 450 ºC can be attributed to the reduction of Ni II species strong interaction with the support [27], [30].

The secondary extension peak observed between 600-800 ºC can be attributed to formation of thermally stable nickel silicate having considerably more difficult reducibility compared to the supported NiO species[32].

The Collective evidence from XRD & TPR studies suggests that Ni was only present in the Ni II species form and that interaction between the metal and support was very strong with almost no support-free Ni II species present.

3.5. Catalytic performance

The impact of reaction temperature was investigated between 200-450ºC. as seen in Fig. 6, The conversion increased rapidly with the increase in temperature up to 400ºC.

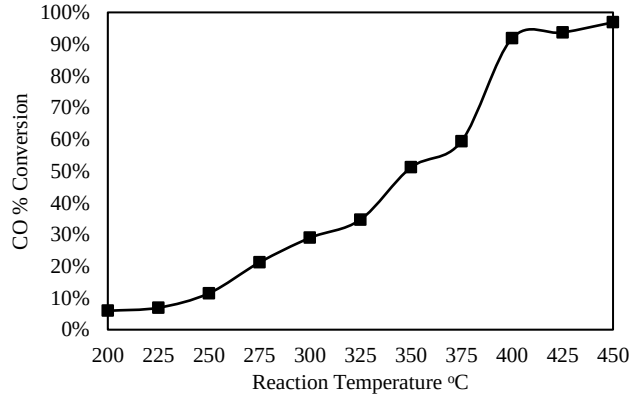

Figure 6. CO Conversion Vs temperature at reaction conditions

Beyond which the conversion kept increasing slightly with the increase in temperature until almost complete conversion was achieved at 450ºC.

Similarly, Fig. 7 suggests that CH_4 selectivity followed an increasing trend with the increase in reaction temperature up to a temperature of 350ºC. Further temperature increase did not yield higher CH_4 selectivity, which could be attributed to thermodynamic equilibrium imitations [1] as well as side reactions like water gas shift[33], [34].

CO_2 selectivity depicted an increasing trend with the increase in temperature up to 350ºC as shown in Fig. 8 where selectivity stagnated at around 20% with further temperature increase. This is due to favorable conversion of CO to CO_2 at higher temperature and low pressure [1]. This is in line with CH_4 selectivity stagnation at temperature above 350ºC.

Despite the high fluidization velocity utilized in the catalytic runs and the aggressive exothermic nature of the reaction, adequate temperature control of the reaction was successfully achieved in the fluidized bed reactor. Moreover, no signs of catalyst deactivation were encountered in over 50 hours of intermittent catalytic testing.

Table 3. Comparison between previous work and current work in CO methanation at a H2:CO ration of 3:1

Catalyst	Reactor Type	T at complete conversion (ºC)	P (atm.)	CH_4 % Selectivity	CO2 % Selectivity
30% NiO/ $LaFeO_3$[4]	Fixed bed	480	10	62%	34%
20% Ni/Al_2O_3 [10]	Fixed bed	400	30	79%	Not reported
this work Ni30	Fluidized bed	450	1	81%	21%

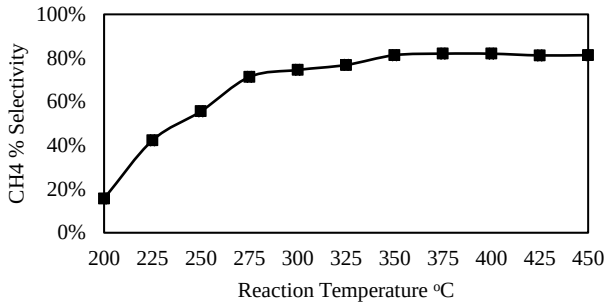

Figure 7. CH4 selectivity Vs temperature at reaction conditions

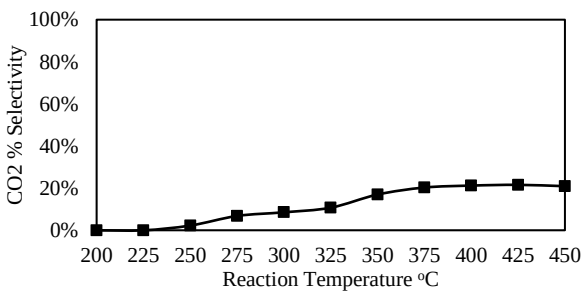

Figure 8. CO2 selectivity Vs temperature at reaction conditions

4. Conclusion

After Nickel oxide was successively supported on rice husk derived silica with a weight concentration of the metal oxide of 30%. Different characterization techniques were used to determine physicochemical properties of the catalyst. The catalyst performance was tested in CO methanation reaction over the temperature range of 200-450ºC and a pressure of 1 bara utilizing a fluidization velocity of $4U_{mf}$. Complete conversion of CO was achieved at a temperature of 450ºC and no indications of catalyst deactivation were observed during over 50 hours of intermittent operation. The semi-pilot scale fluidized bed reactor system proved to be promising in achieving high CO conversion and CH_4 selectivity while providing adequate temperature control over the full range of temperature at relatively high flow rates.

It is recommended to assess the impact of different loading percentages of the metal oxide over the support on catalytic performance. It is recommended to extend the catalytic experiments to determine the effect of different fluidization velocities on the temperature needed for complete conversion of CO. Since CO methanation is a volume decreasing reaction, it is recommended to include the effect of pressure parameter on the catalytic performance in future work.

References

1. J. Gao *et al.*, "A thermodynamic analysis of methanation reactions of carbon oxides for the production of synthetic natural gas," *RSC Advances*, vol. 2, no. 6, pp. 2358–2368, Mar. 2012, doi: 10.1039/c2ra00632d.
2. Z. Chang *et al.*, "Three-dimensional porous Mn–Ni/Al2O3 microspheres for enhanced low temperature CO hydrogenation to produce methane," *International Journal of Hydrogen Energy*, vol. 46, no. 11, pp. 7912–7925, Feb. 2021, doi: 10.1016/j.ijhydene.2020.12.005.
3. M. Tao, X. Meng, Y. Lv, Z. Bian, and Z. Xin, "Effect of impregnation solvent on Ni dispersion and catalytic properties of Ni/SBA-15 for CO methanation reaction," *Fuel*, vol. 165, pp. 289–297, Feb. 2016, doi: 10.1016/j.fuel.2015.10.023.
4. H. Wang, Y. Fang, Y. Liu, and X. Bai, "Perovskite LaFeO3 supported bi-metal catalyst for syngas methanation," *Journal of Natural Gas Chemistry*, vol. 21, no. 6, pp. 745–752, Nov. 2012, doi: 10.1016/S1003-9953(11)60427-1.
5. I. Hussain *et al.*, "Contemporary thrust and emerging prospects of catalytic systems for substitute natural gas production by CO methanation," *Fuel*, vol. 311. Elsevier Ltd, Mar. 01, 2022. doi: 10.1016/j.fuel.2021.122604.
6. J. Gao, Q. Liu, F. Gu, B. Liu, Z. Zhong, and F. Su, "Recent advances in methanation catalysts for the production of synthetic natural gas," *RSC Advances*, vol. 5, no. 29, pp. 22759–22776, 2015, doi: 10.1039/C4RA16114A.
7. A. H. Hatta *et al.*, "A review on recent bimetallic catalyst development for synthetic natural gas production via CO methanation," *International Journal of Hydrogen Energy*, 2021, doi: 10.1016/j.ijhydene.2021.10.213.
8. N. Sánchez-Bastardo, R. Schlögl, and H. Ruland, "Methane Pyrolysis for Zero-Emission Hydrogen Production: A Potential Bridge Technology from Fossil

Fuels to a Renewable and Sustainable Hydrogen Economy," *Industrial and Engineering Chemistry Research*, vol. 60, no. 32, pp. 11855–11881, Aug. 2021, doi: 10.1021/acs.iecr.1c01679.

9. A. Rastegarpanah *et al.*, "Mesoporous Ni/MeO x (Me = Al, Mg, Ti, and Si): Highly efficient catalysts in the decomposition of methane for hydrogen production," *Applied Surface Science*, vol. 478, pp. 581–593, Jun. 2019, doi: 10.1016/j.apsusc.2019.02.009.
10. J. Luo, D. Chen, X. Yue, Y. Feng, and Z. Huang, "Study on syngas methanation over municipal solid waste char supported Ni catalyst," *Fuel*, vol. 303, Nov. 2021, doi: 10.1016/j.fuel.2021.121222.
11. Z. Liu, B. Chu, X. Zhai, Y. Jin, and Y. Cheng, "Total methanation of syngas to synthetic natural gas over Ni catalyst in a micro-channel reactor," *Fuel*, vol. 95, pp. 599–605, May 2012, doi: 10.1016/J.FUEL.2011.12.045.
12. T. T. M. Nguyen, L. Wissing, and M. S. Skjøth-Rasmussen, "High temperature methanation: Catalyst considerations," *Catalysis Today*, vol. 215, pp. 233–238, Oct. 2013, doi: 10.1016/j.cattod.2013.03.035.
13. Y. Liu *et al.*, "Preparation of high-surface-area Ni/α-Al $_2$ O $_3$ catalysts for improved CO methanation," *RSC Advances*, vol. 5, no. 10, pp. 7539–7546, 2015, doi: 10.1039/C4RA13634A.
14. Q. Zhang, Z. Cao, S. Ye, Y. Sha, B. Chen, and H. Zhou, "Mathematical modeling for bubbling fluidized bed CO-methanation reactor incorporating the effect of circulation and particle flows," *Chemical Engineering Science*, vol. 249, Feb. 2022, doi: 10.1016/j.ces.2021.117305.
15. I. Dybkjaer, "Ammonia Production Processes," in *Ammonia*, Berlin, Heidelberg: Springer Berlin Heidelberg, 1995, pp. 199–327. doi: 10.1007/978-3-642-79197-0_6.
16. J. Sehested, S. Dahl, J. Jacobsen, and J. R. Rostrup-Nielsen, "Methanation of CO over Nickel: Mechanism and Kinetics at High H $_2$ /CO Ratios," *The Journal of Physical Chemistry B*, vol. 109, no. 6, pp. 2432–2438, Feb. 2005, doi: 10.1021/jp040239s.
17. J. R. Rostrup-Nielsen and K. Aasberg-Petersen, *Fuel Cell Handbook*, vol. 3. New York: Wiley, 2003.
18. M. L. Pang, W. Y. Shen, and J. Lin, "Enhanced photoluminescence of Ga2O3:Dy3+ phosphor films by Li+ doping," *Journal of Applied Physics*, vol. 97, no. 3, p. 033511, Feb. 2005, doi: 10.1063/1.1849829.
19. M. Wardani, Y. Yulizar, I. Abdullah, and D. O. Bagus Apriandanu, "Synthesis of NiO nanoparticles via green route using *Ageratum conyzoides* L. leaf extract and their catalytic activity," *IOP Conference Series: Materials Science and Engineering*, vol. 509, p. 012077, May 2019, doi: 10.1088/1757-899X/509/1/012077.
20. S. Rakshit, S. Ghosh, S. Chall, S. S. Mati, S. P. Moulik, and S. C. Bhattacharya, "Controlled synthesis of spin glass nickel oxide nanoparticles and evaluation of their potential antimicrobial activity: A cost effective and eco friendly approach," *RSC Advances*, vol. 3, no. 42, p. 19348, 2013, doi: 10.1039/c3ra42628a.
21. M. A. Ermakova and D. Yu. Ermakov, "High-loaded nickel–silica catalysts for hydrogenation, prepared by sol–gel," *Applied Catalysis A: General*, vol. 245, no. 2, pp. 277–288, Jun. 2003, doi: 10.1016/S0926-860X(02)00648-8.
22. R. Haul, "S. J. Gregg, K. S. W. Sing: Adsorption, Surface Area and Porosity. 2. Auflage, Academic Press, London 1982. 303 Seiten, Preis: $ 49.50," *Berichte der Bunsengesellschaft für physikalische Chemie*, vol. 86, no. 10, pp. 957–957, Oct. 1982, doi: 10.1002/bbpc.19820861019.
23. A. Lecloux and J. P. Pirard, "The importance of standard isotherms in the analysis of adsorption isotherms for determining the porous texture of solids," *Journal of Colloid and Interface Science*, vol. 70, no. 2, pp. 265–281, Jun. 1979, doi: 10.1016/0021-9797(79)90031-6.
24. S. Lowell, J. E. Shields, M. A. Thomas, and M. Thommes, *Characterization of Porous Solids and Powders: Surface Area, Pore Size and Density*, vol. 16. Dordrecht: Springer Netherlands, 2004. doi: 10.1007/978-1-4020-2303-3.
25. W. Trisunaryanti, E. Suarsih, Triyono, and I. I. Falah, "Well-dispersed nickel nanoparticles on the external and internal surfaces of SBA-15 for hydrocracking of pyrolyzed α-cellulose," *RSC Advances*, vol. 9, no. 3, pp. 1230–1237, 2019, doi: 10.1039/c8ra09034c.
26. C. Paramesti *et al.*, "The influence of metal loading amount on ni/mesoporous silica extracted from lapindo mud templated by ctab for conversion of waste cooking oil into biofuel," *Bulletin of Chemical Reaction Engineering & Catalysis*, vol. 16, no. 1, pp. 22–30, 2021, doi: 10.9767/BCREC.16.1.9442.22-30.
27. S. R. Kirumakki, B. G. Shpeizer, G. V. Sagar, K. V. R. Chary, and A. Clearfield, "Hydrogenation of Naphthalene over NiO/SiO2-Al2O3 catalysts: Structure-activity correlation," *Journal of Catalysis*, vol. 242, no. 2, pp. 319–331, Sep. 2006, doi: 10.1016/j.jcat.2006.06.014.
28. J. M. Rynkowski, T. Paryjczak, and M. Lenik, "On the nature of oxidic nickel phases in NiO/y-AI 20a catalysts 73," 1993.
29. S. J. Tauster, "Strong metal-support interactions," *Accounts of Chemical Research*, vol. 20, no. 11, pp. 389–394, Nov. 1987, doi: 10.1021/ar00143a001.
30. Y. Abdelbaki *et al.*, "The nickel-support interaction as determining factor of the selectivity to ethylene in the oxidative dehydrogenation of ethane over nickel oxide/alumina catalysts," *Applied Catalysis A: General*, vol. 623, Aug. 2021, doi: 10.1016/j.apcata.2021.118242.
31. B. Mile, D. Stirling, M. A. Zammi, and M. Webb, "TFR S'I'UDDZS OF THE EFFECTS OF PREPARATION CONDITIONS ON SUFFORTED NICKEL CATALYSTS," 1990.
32. M.-T. Tsay and F.-W. Chang, "Characterization of rice husk ash-supported nickel catalysts prepared by ion exchange," 2000.
33. Y. Han, Y. Quan, P. Hao, J. Zhao, and J. Ren, "Highly anti-sintering and anti-coking ordered mesoporous silica carbide supported nickel catalyst for high temperature CO methanation," *Fuel*, vol. 257, Dec. 2019, doi: 10.1016/j.fuel.2019.116006.
34. M. v. Konishcheva, D. I. Potemkin, P. v. Snytnikov, O. A. Stonkus, V. D. Belyaev, and V. A. Sobyanin, "The insights into chlorine doping effect on performance of ceria supported nickel catalysts for selective CO methanation," *Applied Catalysis B: Environmental*, vol. 221, pp. 413–421, 2018, doi: 10.1016/j.apcatb.2017.09.038.